JOURNAL OF COMPUTATIONAL PHYSICS 107, 378–387 (1993)

# A Fast Algorithm to Compute the Wave-Scattering Solution of a Large Strip*

W. C. CHEW AND C. C. LU

*Electromagnetics Laboratory, Department of Electrical and Computer Engineering, University of Illinois, Urbana, Illinois 61801*

Received August 7, 1991; revised May 28, 1992

A truncated, nonuniform, finite array of strips does not have a closed form solution. Using translational symmetry, a recursive algorithm that calculates the scattering solution with $N \log^2 N$ computational complexity is described. First, the algorithm is validated with the method of moments for both the TM-to-$z$ and TE-to-$z$ polarizations. Then the scattering solution from a large strip is calculated for both TE and TM polarizations. The current distribution for the TE polarization shows small-length-scale oscillations not present in the TM polarization.


## 1. INTRODUCTION

The scattering of waves by large objects and structures is important in a number of applications. Such scattering solutions could be used for computer-aided engineering. However, the computer solution of large structures consumes exorbitant amounts of computer time and computer memory. Recently, it has been demonstrated that algorithms for scattering solutions with reduced computational complexity can be derived using a recursive structure [1–10]. The reason for the reduction in computational complexity has been traced to the use of addition theorems or translational matrices which are used to change the coordinates of the wave functions describing the scattered field. The translation matrices are the representation of the translation group [11, 12]. Hence, the product of two translation matrices is still a translation matrix exhibiting the closure property of a group.

In the addition theorem for cylindrical harmonics, the basis for the representation of the translation group is the Bessel function. However, since the translation group is Abelian, a simpler group representation is possible [12]. If plane waves are used as a basis for the translation group, a simple representation results. In this paper, we shall demonstrate the use of a plane-wave basis for the expansion of the scattered field by a finite, nonuniform array of strips. This is equivalent to the use of plane waves as a basis for the representation of the translation group, which reduces the translation matrices to diagonal matrices which are easy to compute. Eventually, it leads to an algorithm with a computational complexity of $O(N \log^2 N)$ which is much faster than any other method to solve this scattering problem.

The problem of wave scattering by strips, other than being a canonical problem, has many practical applications. Hence, it has been investigated by many workers [13–16]. However, due to the high complexity of the previous methods to solve this problem, only relatively smaller-size problems have currently been solved. The algorithm described here will have two advantages: First, it can solve for the scattering solution from any array of coplanar strips regardless of the nonuniformity of the array. Second, it has a reduced computational complexity compared to previous methods of solving this problem. The limitation at this point is its application only to a coplanar array of parallel strips. Hopefully, future research work will lift this restriction. Also, with a slight modification, the present formulation can be extended to that for an array of resistive strips.

In the following, we will first describe the plane-wave representation of the two-dimensional Green's function. Then, using the point-matching technique, the scattering solution from one single substrip is described. Later, a forward recursive algorithm and a backward recursive algorithm are given that yield the solution of scattering by $N$ substrips. Then the computational complexity and memory requirement of the algorithm is analyzed. Finally, the algorithm is validated with the method of moments and tested with some numerical simulations of large strips.

## 2. PLANE-WAVE EXPANSION OF THE GREEN'S FUNCTION

Given an array of strips, it can be decomposed into $N$ substrips; the width of each substrip is much smaller than a wavelength. Hence, the problem of scattering by an array of

* This work is supported by National Science Foundation under Grant NSF ECS-85-25891 and Office of Naval Research under Grant N00014-89-J1286.

0021-9991/93 $5.00

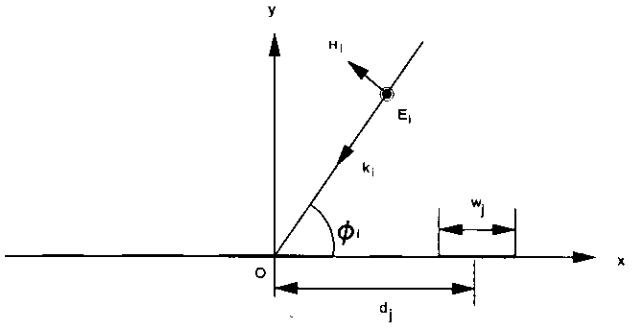


FIG. 1. Geometrical configuration of wave scattering by a finite, nonuniform array of strips.

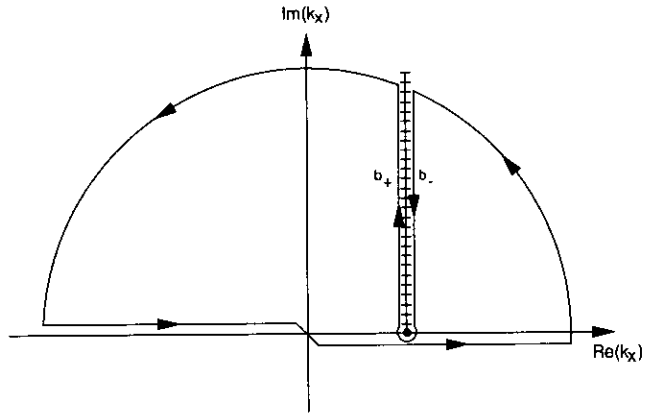


FIG. 2. Deformation of the Fourier inversion contour to the vertical branch cut. The vertical branch cut in this case is also the steepest descent path.

strips is reduced to the problem of scattering by $N$ substrips, some of which are touching and some of which are not touching. Hence, the geometry of the scattering problem is shown in Fig. 1. It consists of $N$ parallel and coplanar conducting substrips, each of which has a width of $w_j$. For simplicity, we shall omit the subscript $j$ in the subsequent discussion. The center of each substrip is denoted by $x = d_i$ for $i = 1, ..., N$, and $N$ is the total number of substrips.

First, we shall study wave scattering by a single substrip when illuminated by an incident wave. For instance, in the TM-to-$z$ case where the geometry is $z$ invariant, the incident field is characterized by the $z$ component of the electric field which is $E_z^i$. If the induced current on the strip is $J_z$, which is also $z$ invariant, then the scattered field can be derived as

$$E_z^s = i\omega\mu \int_{-w/2}^{w/2} G_0(\boldsymbol{\rho} - \boldsymbol{\rho}')\, J_z(x')\, dx', \tag{1}$$

where $\boldsymbol{\rho} = \hat{x}x + \hat{y}y$. Here, $G_0(\boldsymbol{\rho} - \boldsymbol{\rho}') = (i/4)H_0^{(1)}(k|\boldsymbol{\rho} - \boldsymbol{\rho}'|)$ is the free-space Green's function in two dimensions [17], and $H_0^{(1)}(x)$ is the zeroth-order Hankel function of the first kind. Here $e^{-i\omega t}$ time dependence is assumed.

The Hankel function can be expanded as a spectral integral as [5, p. 59]

$$H_0^{(1)}(k|\boldsymbol{\rho} - \boldsymbol{\rho}'|) = \frac{1}{\pi} \int_{-\infty}^{\infty} dk_x \frac{1}{k_y} e^{ik_x(x-x') + ik_y|y-y'|}, \tag{2}$$

where $k_y = \sqrt{k^2 - k_x^2}$, and an appropriate branch of the square root is chosen in the above integral to satisfy the radiation condition [5]. When $x - x'$ is large, the oscillatory nature of the integrand makes the evaluation of the integral difficult. To overcome this problem, the path of integration is deformed to the steepest descent path. For coplanar strips, without loss of generality, we can assume $y = y' = 0$. Hence, the steepest descent path is just the vertical branch cut as shown in Fig. 2 [18]. When $x > x'$, the integration path can be deformed to $b_-$ and $b_+$, so that after combining the integration over $b_-$ and $b_+$ we have

$$H_0^{(1)}(k|x - x'|) = e^{ik|x-x'|} \int_0^{+\infty} ds\, f(s)\, e^{-s|x-x'|}, \tag{3}$$

where

$$f(s) = \frac{2}{\pi[s^2 + 2iks]^{1/2}}. \tag{3a}$$

The above is a function of $|x - x'|$ because the result must be an even function of $|x - x'|$. Now, the above integral converges exponentially fast as a result of the exponential decay of the integrand for increasing $s$.

When $|x - x'| \to \infty$, most of the contribution to the integral will come from values of $s < 1/|x - x'|$. Moreover, the above could be approximated by a discrete summation using, e.g., trapezoidal integration or Gaussian quadrature rule. Hence,

$$H_0^{(1)}(k|x - x'|) \cong \sum_{m=1}^{M} h_m e^{-u_m|x-x'|}, \tag{4}$$

where

$$u_m = -ik + s_m$$

and $h_m$ is the appropriately weighted value of the integrand at $s_m$.

The sampling points in approximating the integral (2) need not be evenly distributed. The sampling intervals can be distributed with the finest sampling points close to $s = 0$ and increasingly coarser sampling points when $s \to \infty$. For instance, one can let $s_2 = \alpha s_1$, $s_i = \alpha s_{i-1}$, so that $s_M = \alpha^{M-1} s_1$, where $\alpha > 1$.

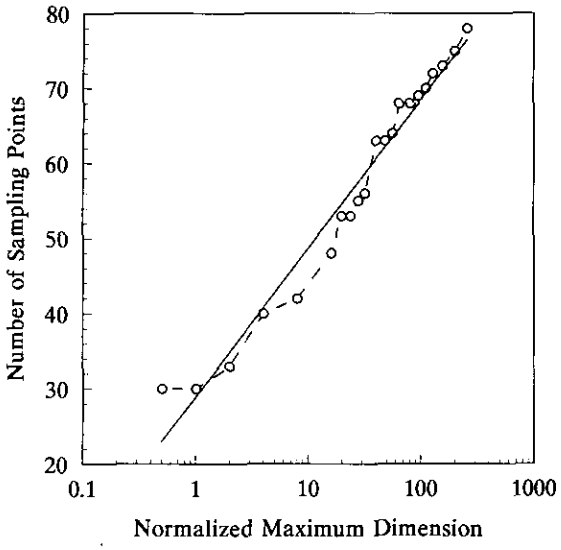


FIG. 3. The increase in the number of sampling points with the maximum dimension of the array on a semilog plot.

The grid points have to be chosen so that (4) is valid for a range of values of $|x-x'|$. The integrand is discretized over the interval $[0, s_M]$, where $s_1$ is determined by the largest value of $|x-x'|$ and $s_M$ is determined by the smallest value of $|x-x'|$. In other words, $s_1 = c_1/|x-x'|_{\max}$, and $s_M = c_M/|x-x'|_{\min}$. Hence, $s_M/s_1 \sim |x-x'|_{\max}/|x-x'|_{\min}$. Since $s_M/s_1 = \alpha^{M-1}$, we have $M \sim \ln\{|x-x'|_{\max}\} - \ln\{|x-x'|_{\min}\}$. Since $|x-x'|_{\min} \approx w$, the number of sampling points $M$ needed to approximate the integral is proportional to $\log\{|x-x'|_{\max}\}$. Figure 3 shows a semilog plot of the increase in the number of sampling points as a function of the maximum size of the array of strips to maintain the same accuracy in the integration. It is seen that $M$ is proportional to $\ln(kW)$, where $W$ is the maximum width of the array.

In Eq. (4), we have an efficient representation of the Green's function of the problem in terms of a plane-wave basis which has translational symmetry. This translational symmetry can then be later exploited to derive a recursive algorithm with reduced computational complexity.

## 3. T MATRIX FOR A SINGLE STRIP

Even though T matrices have been defined when cylindrical wave harmonics or spherical wave harmonics are used as a basis [19, 20], the definition can be extended to the case when the basis is a plane wave.

### 3.1. *TM case*

For TM-to-$z$ fields with a $z$-invariant geometry, the electric field is $z$ polarized and the induced current on the strip is $z$ directed. Consider a single substrip, centered at $x=0$, and whose dimension $kw$ is small so that the induced current $J_z$ on it can be approximated by a constant. Then the scattered field is

$$E_z^s(x) = \frac{-\omega\mu J_z}{4}\int_{-w/2}^{w/2} H_0^{(1)}(k\,|x-x'|)\,dx' \tag{5}$$

on the $y=0$ plane. Substituting the approximation (4) into (5), we have for $|x| > w/2$, that

$$E_z^s(x) = J_z \sum_{m=1}^{M} b_m e^{-u_m|x|} = \boldsymbol{\psi}_s^t(x)\cdot\mathbf{b}J_z, \tag{6}$$

where

$$b_m = \frac{-\omega\mu}{4} h_m \int_{-w/2}^{w/2} e^{u_m x'}\,dx', \tag{6a}$$

$$\mathbf{b} = [b_1, b_2, \ldots, b_M]^t, \tag{6b}$$

and

$$\boldsymbol{\psi}_{s\pm}(x) = [e^{\mp u_1 x}, e^{\mp u_2 x}, \ldots, e^{\mp u_M x}]^t. \tag{6c}$$

The subscript $\pm$ indicates the scattered fields to the right and to the left of the substrip, respectively. This sign will be dropped if there is no ambiguity, e.g., in the case when the scattered field is an even symmetric function of $x$.

Hence, the scattered field of a substrip is expanded in terms of a plane-wave basis on the $y=0$ plane. When many substrips are present, these plane waves given in (6), plus the plane wave from an external source can be considered the incident field on a substrip. Hence, the incident wave on a substrip can be expanded in terms of the basis

$$e^{ik_{ix}x}, \text{ and } e^{\pm u_m x}, \qquad m = 1, 2, \ldots, M, \tag{7}$$

where $k_{ix}$ is the $x$ component of the incident wave $k$-vector. Therefore, it is reasonable to assume an incident wave vector of the form

$$\boldsymbol{\psi}_{i\pm}(x) = [e^{ik_{ix}x}, e^{\pm u_1 x}, e^{\pm u_2 x}, \ldots, e^{\pm u_M x}]^t. \tag{8}$$

The subscript $\pm$ indicates a wave incident from the right and left, respectively. It will be dropped if the scattering property of the strip is independent of the direction of the incident wave. Consequently, the incident field impinging on a substrip can be written as $\boldsymbol{\psi}_i^t(x)\cdot\mathbf{a}$ without loss of generality.

Imposing the boundary condition by point matching [21] at $x=0$, the center of the substrip, we have

$$J_z \frac{\omega\mu}{4}\int_{-w/2}^{w/2} H_0^{(1)}(k\,|x'|)\,dx' = \boldsymbol{\psi}_i^t(0)\cdot\mathbf{a}. \tag{9}$$

Consequently, $J_z$ could be solved for and substituted into (6) to yield

$$E_z^s(x) = \boldsymbol{\psi}_s^t(x) \cdot \mathbf{b}\mathbf{f}^t \cdot \mathbf{a} = \boldsymbol{\psi}_s^t(x) \cdot \bar{\mathbf{T}} \cdot \mathbf{a}, \tag{10}$$

where

$$\mathbf{f}^t = \left[ \frac{\omega\mu}{4} \int_{-w/2}^{w/2} H_0^{(1)}(k\,|x'|) \right]^{-1} \boldsymbol{\psi}_i^t(0) \tag{10a}$$

and

$$\bar{\mathbf{T}} = \mathbf{b}\mathbf{f}^t. \tag{10b}$$

The above gives the T matrix that relates the scattered field amplitudes to the incident field amplitudes for a TM-polarized incident field on a single substrip.

### 3.2. *TE Case*

In this polarization, the electric field is polarized in the $xy$ plane. The induced current on the strip is in the $x$ direction. Hence, the current cannot be assumed constant anymore on each substrip. In this case, we choose a trapezoidal function as a basis for each substrip. As a result, the charge distribution on the substrip will consist of a pulse function plus two delta functions as shown in Fig. 4. From Maxwell's equation, the scattered field consists of two terms, one resulting from the current on the substrip while the other is from the charge. In other words,

$$E_x^s = i\omega\mu \int_{-w/2}^{w/2} J_{sx} G_0(\boldsymbol{\rho} - \boldsymbol{\rho}')\, dx' + \frac{i\omega\mu}{k^2} \frac{\partial}{\partial x} \int_{-w/2}^{w/2} i\omega\rho_s G_0(\boldsymbol{\rho} - \boldsymbol{\rho}')\, dx', \tag{11}$$

where $J_{sx}$ is the $x$ component of the surface current on the substrip while $\rho_s = (1/i\omega)(dJ_{sx}/dx)$ is the surface charge density on the substrip.

By letting $J_{sx} = \sum_{i=1}^{2} I_i t_i(x)$, where $t_1(x)$ is a half-triangular function at $-w/2$, and $t_2(x)$ is the mirror image of $t_1(x)$, Eq. (11) at $y = y' = 0$ can be expressed as

$$E_x^s(x) = I_1 C_1(x) + I_2 C_2(x), \tag{12}$$

where

$$C_i(x) = i\omega\mu \left[ \int_{-w/2}^{w/2} t_i(x')\, G_0(x - x')\, dx' + \frac{1}{k^2} \frac{\partial}{\partial x} \int_{-w/2}^{w/2} \times \left( \frac{\partial}{\partial x'} t_i(x') \right) G_0(x - x')\, dx' \right]. \tag{12a}$$

When the approximation (4) for the Green's function is substituted into (12), we can show that

$$E_x^s(x) = \boldsymbol{\psi}_{s\pm}^t(x) \cdot \bar{\mathbf{b}}^{(\pm)} \cdot \mathbf{I}, \qquad |x| > w/2, \tag{13}$$

where $\mathbf{I}$ is a two-component column vector containing $I_1$ and $I_2$, and $\bar{\mathbf{b}}_{\pm}$ is a $M \times 2$ matrix. The superscript $\pm$ is used in $\bar{\mathbf{b}}^{(\pm)}$ because its values for the left-going and the right-going scattered fields are different due to the asymmetry in the basis functions.

The incident wave impinging on the strip could be from the right or from the left, which can be written as $E_x^i(x) = \boldsymbol{\psi}_{i\pm}^t(x) \cdot \mathbf{a}$. To point match on the surface of the strip, we have to use Eq. (12) for $E_x^s$. The resultant point-matched equation can be expressed as

$$E_x^s(x_j) = \sum_{i=1}^{2} I_i C_i(x_j) = -E_x^i(x_j), \tag{14}$$

where $x_1 = -b$, $x_2 = +b$ are match points on the substrip. Since $E_x^i = \boldsymbol{\psi}_{i\pm}^t(x) \cdot \mathbf{a}$, the above is of the form

$$\sum_{i=1}^{2} C_{ji} I_i = -\boldsymbol{\psi}_{i\pm}^t(x_j) \cdot \mathbf{a}, \qquad j = 1, 2, \tag{15}$$

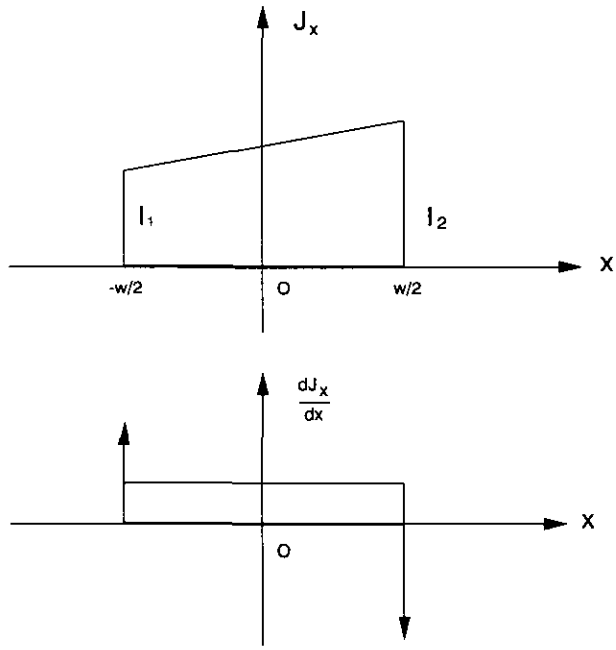


**FIG. 4.** The current and charge distributions ($\sim \partial J_x/\partial x$) on a subtrip for the TE-polarized incident wave.

where, $C_{ji} = C_i(x_j)$. The above could be solved to yield

$$\mathbf{I} = -\bar{C}^{-1} \cdot \begin{bmatrix} \psi^t_{i\pm}(x_1) \\ \psi^t_{i\pm}(x_2) \end{bmatrix} \cdot \mathbf{a} = \bar{\mathbf{f}}^{t(\pm)} \cdot \mathbf{a}. \tag{16}$$

Note that $\mathbf{I}$ is dependent on the direction of the incident field. Using (16) in (13), we have

$$E^s_x(x) = \psi^t_{s\pm}(x) \cdot \bar{\mathbf{b}}^{(\pm)} \bar{\mathbf{f}}^{t(\pm)} \cdot \mathbf{a} = \psi^t_{s\pm}(x) \cdot \bar{\mathbf{T}}^{(\pm,\pm)} \cdot \mathbf{a}. \tag{17}$$

The double superscripts on the T matrix indicate that it is sensitive to the directions of both the incident and the scattered fields.

## 4. THE FORWARD RECURSIVE ALGORITHM

Given the scattering solution of each substrip, a recursive algorithm can be derived such that the $(n+1)$-substrip solution can be found from the $n$-substrip solution [4, 5]. In this manner, the $N$-substrip solution could be recursively constructed from the one-substrip solution.

When $n$ substrips are present, the total field could be written as

$$\phi(x, y=0) = \overbrace{\psi^t_{i+}(x_0) \cdot \mathbf{a}}^{\text{incident}} + \overbrace{\psi^t_{s+}(x_0) \cdot \bar{\tau}_{(n)} \cdot \mathbf{a}}^{\text{scattered}}, \tag{18}$$

where $x_0$ is the $x$ coordinate with respect to a global or zeroth coordinate system. The above expression is only valid for $x_0$ to the right of the $n$ substrips, since the scattered field is travelling to the right and the incident field is coming from the right. Since the $n$ substrips may not have reflection symmetry, the scattered field to the right may not be the same as the scattered field to the left for the same incident field. Also, its response to the incident field from the right may not be the same as to that from the left. Hence, there are four possible combinations of the incident directions and observation directions.

When the $(n+1)$th substrip is added to the right of the $n$ substrips, the total field could be written as

$$\phi(x, y=0) = \psi^t_{i+}(x_0) \cdot \mathbf{a} + \psi^t_{s+}(x_0) \cdot \bar{\tau}_{n(n+1)} \cdot \mathbf{a} + \psi^t_{s\pm}(x_{n+1}) \cdot \bar{\mathbf{K}}^{(\pm)}_{n+1(n+1)} \cdot \mathbf{a}. \tag{19}$$

The subscript $\pm$ on $\psi^t_s$ is used in the last term to indicate that the model expansion is valid both to the right and to the left of the $(n+1)$th substrip. The superscript $(\pm)$ on $\bar{\mathbf{K}}$ indicates its dependence on the two possible incident field directions.

The translation matrix similar to Ref. [1–6] could be used to express the scattered wave of the last term in (19) in terms of the zeroth coordinates yielding

$$\phi(x, y=0) = \psi^t_{i+}(x_0) \cdot \mathbf{a} + \psi^t_{s+}(x_0) \cdot \bar{\tau}_{n(n+1)} \cdot \mathbf{a} + \psi^t_{i+}(x_0) \cdot \bar{\alpha}_{0,n+1} \cdot \bar{\mathbf{K}}^{(-)}_{n+1(n+1)} \cdot \mathbf{a}. \tag{20}$$

In the above, note that the third term has the same form (except for a different amplitude) as the first term—the incident wave from outside the strip array. In fact, the third term can be thought of as an incident wave, due to a wave scattered off the $(n+1)$th substrip, on the $n$-substrip array. Consequently, regarding the first and the third terms as the incident field on the $n$ substrips, and the second term as the scattered field from the $n$ substrips, we have the relationship

$$\bar{\tau}_{n(n+1)} = \tau_{(n)} \cdot [\bar{\mathbf{I}} + \bar{\alpha}_{0,n+1} \cdot \bar{\mathbf{K}}^{(-)}_{n+1(n+1)}], \tag{21}$$

where $\bar{\tau}_{n(n+1)}$ is the aggregate $T$ matrix for the $n$ substrips in the presence of the $n+1$ substrips.

Similarly, by shifting the coordinates of the first two terms in (19) to the coordinates of the $(n+1)$th substrip, we have

$$\phi(x, y=0) = \psi^t_{i+}(x_{n+1}) \cdot \bar{\beta}_{n+1,0} \cdot \mathbf{a} + \psi^t_{i-}(x_{n+1}) \cdot \bar{\alpha}_{n+1,0} \cdot \bar{\tau}_{n(n+1)} \cdot \mathbf{a} + \psi^t_{s\pm}(x_{n+1}) \cdot \bar{\mathbf{K}}^{(\pm)}_{n+1(n+1)} \cdot \mathbf{a}. \tag{22}$$

Now, the first two terms in (22) resemble the incident wave impinging on the $(n+1)$th substrip. Hence, the third term, which is the scattered field from a single substrip, can be related to the first two terms via the isolated-scatterer T matrix derived in (10) and (17). In this case, the incident fields on the $(n+1)$th substrip are coming from both the right and the left sides. Hence, we deduce the relationship

$$\bar{\mathbf{K}}^{(\pm)}_{n+1(n+1)} = \bar{\mathbf{T}}^{(\pm,+)}_{n+1(1)} \cdot \bar{\beta}_{n+1,0} + \bar{\mathbf{T}}^{(\pm,-)}_{n+1(1)} \cdot \bar{\alpha}_{n+1,0} \cdot \bar{\tau}_{n(n+1)}. \tag{23}$$

However, note that the T-matrix solution derived in (10) is independent of the directions of the incident wave. Therefore, the $\pm$ sign may be removed for TM polarization.

Solving (21) and (23) for $\bar{\mathbf{K}}^{(-)}_{n+1(n+1)}$ yields

$$\bar{\mathbf{K}}^{(-)}_{n+1(n+1)} = [\bar{\mathbf{I}} - \bar{\mathbf{T}}^{(-,-)}_{n+1(1)} \cdot \bar{\alpha}_{n+1,0} \cdot \bar{\tau}_{(n)} \cdot \bar{\alpha}_{0,n+1}]^{-1} \times [\bar{\mathbf{T}}^{(-,+)}_{n+1(1)} \cdot \bar{\beta}_{n+1,0} + \bar{\mathbf{T}}^{(-,-)}_{n+1(1)} \cdot \bar{\alpha}_{n+1,0} \cdot \bar{\tau}_{(n)}]. \tag{24}$$

Using the property (10b) that $\bar{\mathbf{T}}^{(\pm,\pm)}_{n+1(1)} = \bar{\mathbf{b}}^{(\pm)}_{n+1} \bar{\mathbf{f}}^{t(\pm)}_{n+1(1)}$, the above could be simplified to

$$\bar{\mathbf{K}}^{(-)}_{n+1(n+1)} = \bar{\mathbf{b}}^{(-)}_{n+1} \bar{\mathbf{f}}^t_{n+1(n+1)}, \tag{25}$$

where

$$\bar{\mathbf{f}}^{t}_{n+1(n+1)} = \Big(\underbrace{\bar{\mathbf{I}}}_{2\times 2} - \underbrace{\bar{\mathbf{f}}^{t(-)}_{n+1(1)}}_{2\times(M+1)} \cdot \underbrace{\bar{\boldsymbol{\alpha}}_{n+1,0}}_{(M+1)\times M} \cdot \underbrace{\bar{\boldsymbol{\tau}}_{(n)}}_{M\times(M+1)} \cdot \underbrace{\bar{\boldsymbol{\alpha}}_{0,n+1}}_{(M+1)\times M} \cdot \underbrace{\bar{\mathbf{b}}_{n+1}}_{M\times 2}\Big)^{-1} \cdot \Big[\underbrace{\bar{\mathbf{f}}^{t(+)}_{n+1(1)}}_{2\times(M+1)} \cdot \underbrace{\bar{\boldsymbol{\beta}}_{n+1,0}}_{(M+1)\times(M+1)} + \underbrace{\bar{\mathbf{f}}^{t(-)}_{n+1(1)}}_{2\times(M+1)} \cdot \underbrace{\bar{\boldsymbol{\alpha}}_{n+1,0}}_{(M+1)\times M} \cdot \underbrace{\bar{\boldsymbol{\tau}}_{(n)}}_{M\times(M+1)}\Big]. \tag{25a}$$

Note that the number of columns in $\bar{\mathbf{b}}$ and $\bar{\mathbf{f}}$ are one for the TM case and two for the TE case. Hence, in (25a), the order of the matrix to be inverted is at most $2\times 2$.

Once $\bar{\mathbf{K}}^{(-)}_{n+1(n+1)}$ is known, $\bar{\boldsymbol{\tau}}_{n(n+1)}$ can be found from (21). An aggregate T matrix [4] could be defined for $(n+1)$ substrips as

$$\bar{\boldsymbol{\tau}}_{(n+1)} = \bar{\boldsymbol{\tau}}_{n(n+1)} + \bar{\boldsymbol{\beta}}_{0,n+1} \cdot \bar{\mathbf{K}}_{n+1(n+1)} = \underbrace{\bar{\boldsymbol{\tau}}_{(n)}}_{M\times(M+1)} + \underbrace{\bar{\boldsymbol{\tau}}_{(n)}}_{M\times(M+1)} \cdot \underbrace{\bar{\boldsymbol{\alpha}}_{0,n+1}}_{(M+1)\times M} \cdot \underbrace{\bar{\mathbf{b}}_{n+1}}_{M\times 2} \underbrace{\bar{\mathbf{f}}^{t}_{n+1(n+1)}}_{2\times(M+1)} + \underbrace{\bar{\boldsymbol{\beta}}_{0,n+1}}_{M\times M} \cdot \underbrace{\bar{\mathbf{b}}_{n+1}}_{M\times 2} \underbrace{\bar{\mathbf{f}}^{t}_{n+1(n+1)}}_{2\times(M+1)}. \tag{26}$$

The dimensions of the matrices are shown by over- and under-braces in (25a) and (26) for the TE case.

In the above, assuming that the $j$th substrip is always to the right of the zeroth coordinate system, then,

$$\bar{\boldsymbol{\beta}}_{j0} = \operatorname{diag}[e^{ik_{ix}d_{j0}}, e^{u_1 d_{j0}}, \ldots, e^{u_M d_{j0}}]_{(M+1)\times(M+1)}, \tag{27a}$$

$$\bar{\boldsymbol{\beta}}_{0j} = \operatorname{diag}[e^{u_1 d_{j0}}, e^{u_2 d_{j0}}, \ldots, e^{u_M d_{j0}}]_{M\times M}, \tag{27b}$$

and

$$\bar{\boldsymbol{\alpha}}_{0j} = \bar{\boldsymbol{\alpha}}_{j0} = \begin{bmatrix} O_{1\times M} \\ \operatorname{diag}(e^{-u_1 d_{j0}}, e^{-u_2 d_{j0}}, \ldots, e^{-u_M d_{j0}})_{M\times M} \end{bmatrix}_{(M+1)\times M}. \tag{27c}$$

Note that the translation matrices are diagonal or quasidiagonal because of the Abelian property of the translation group.

When the strip becomes very wide, it is expedient to shift the origin of the zeroth coordinate system to the center of the $n$th substrip. This will avoid the cancellation of exponentially large and exponentially small numbers in the recursive method.

## 5. BACKWARD RECURSION FORMULAS

In order to derive the current distribution on the strip, backward recursion formulas similar to those in [4] need to be derived. In this case, it is more pertinent to write the total field after forward recursion as

$$\phi = \boldsymbol{\psi}^{t}_{i+}(x_0) \cdot \mathbf{a} + \sum_{i=1}^{N} \boldsymbol{\psi}^{t}_{s-}(x_i) \cdot \bar{\mathbf{K}}^{(-)}_{i(N)} \cdot \mathbf{a}, \tag{28}$$

where the scattered field from each substrip is expressed in its self-coordinates. Using $\bar{\mathbf{K}}^{(-)}_{j(j)}$, $j=1, \ldots, N$, from the forward recursion, we can derive backward recursion formulas for $\bar{\mathbf{K}}^{(-)}_{i(N)}$ as in [4]. They are

$$\bar{\tilde{\boldsymbol{\tau}}}_{(0)} = \bar{\boldsymbol{\alpha}}_{0N} \cdot \bar{\mathbf{K}}^{(-)}_{N(N)} \tag{29a}$$

$$\bar{\mathbf{K}}^{(-)}_{N-i(N)} = \bar{\mathbf{K}}^{(-)}_{N-i(N-i)} \cdot [\bar{\mathbf{I}} + \bar{\tilde{\boldsymbol{\tau}}}_{(i-1)}], \quad i = 1, \ldots, N-1, \tag{29b}$$

$$\bar{\tilde{\boldsymbol{\tau}}}_{(i)} = \bar{\tilde{\boldsymbol{\tau}}}_{(i-1)} + \bar{\boldsymbol{\alpha}}_{0,N-i} \cdot \bar{\mathbf{K}}^{(-)}_{N-i(N)}, \quad i = 1, \ldots, N-1. \tag{29c}$$

Using (29a) as the initial condition, and the value of $\bar{\mathbf{K}}^{(-)}_{j(j)}$, $j=1, \ldots, N$, the above allows one to find $\bar{\mathbf{K}}^{(-)}_{i(N)}$, $i=1, \ldots, N$. With $\bar{\mathbf{K}}^{(-)}_{i(N)}$ known, the current distribution on the strips could be found. Once the current distribution is known, the field could be easily found, e.g., by the FFT method. The computational cost and memory requirement of the above formulas can be reduced by using the form (25) for $\bar{\mathbf{K}}^{(-)}_{i(N)}$.

## 6. COMPUTATIONAL COMPLEXITY

It can be seen from Eqs. (25) and (26) that at each recursive step, $O(M^2)$ multiplications are needed to find $\mathbf{f}_{n+1(n+1)}$ and $\bar{\boldsymbol{\tau}}_{(n+1)}$. After $N$ recursive steps, the total number of floating point operation is $O(NM^2)$. Since $M \propto \ln kd$, where $d$ is the largest dimension of the array, and $kd \sim N$, we have $M \sim \ln N$. Consequently, the computational complexity of this algorithm is $O(N \log^2 N)$. The memory requirement can be shown to be $O(N \log N)$. The above analysis is for one incident plane wave. If $N$ incident plane waves are assumed, an analysis of the computational complexity yields $O(N^2 \log N)$. The memory requirement is $O(N^2)$. This algorithm is of reduced computational complexity compared to the method of moments, conjugate gradient, or conjugate gradient FFT methods applied to this problem [22–25].

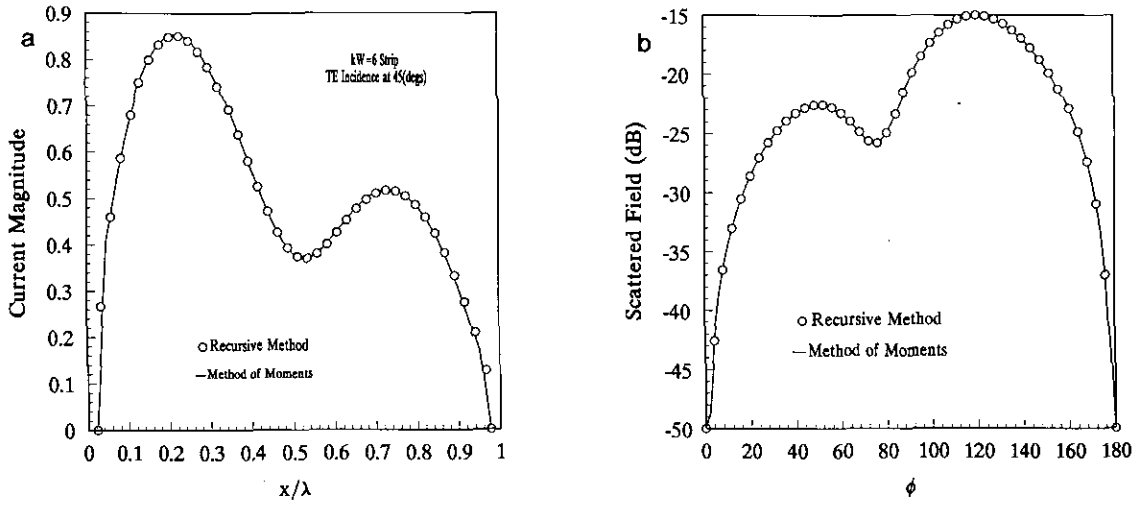


FIG. 5. A single $kW = 6$ strip illuminated by a TM plane wave incident at 45° and comparison with the method of moments: (a) The current distribution on the strip. (b) The scattered far field.

## 7. NUMERICAL RESULTS

In the following results, the TE simulations are performed with about 40 substrips per wavelength while the TM simulations are performed with about 20 substrips per wavelength in order to obtain good current distributions on the strips. If only far fields are needed, sampling rates can be reduced by a factor of two. All substrips are assumed to be of the same width $w$. The current distributions are normalized by the factor $4\,|\mathbf{H}|/(kw)$ for the TM case and $4\,|\mathbf{H}|$ for the TE case. All computations are performed on a SUN 4/110. The scattered far field for the TM case is normalized by the factor $\sqrt{2\pi\rho}$, while for the TE case it is normalized by the factor $\sqrt{8\pi\rho\lambda/W}$, where $W$ is the width of the strip.

Figure 5a shows the current distribution on a single strip whose width is such that $kW = 6$. The strip is illuminated by a TE plane wave at 45°. The comparison with the method of moments on the current distribution shows good agreement. Figure 5b shows the calculated scattered far field displaying good agreement with the method of moments.

Figure 6a shows the calculated current distribution on a strip illuminated by a TM plane wave at normal incidence with $kW = 15.7$. It shows good agreement with the method of moments. Figure 6b shows the corresponding calculated scattered far field showing good agreement with the method of moments.

Figure 7a shows the current distribution on a 20-wavelength wide strip illuminated by a normally incident

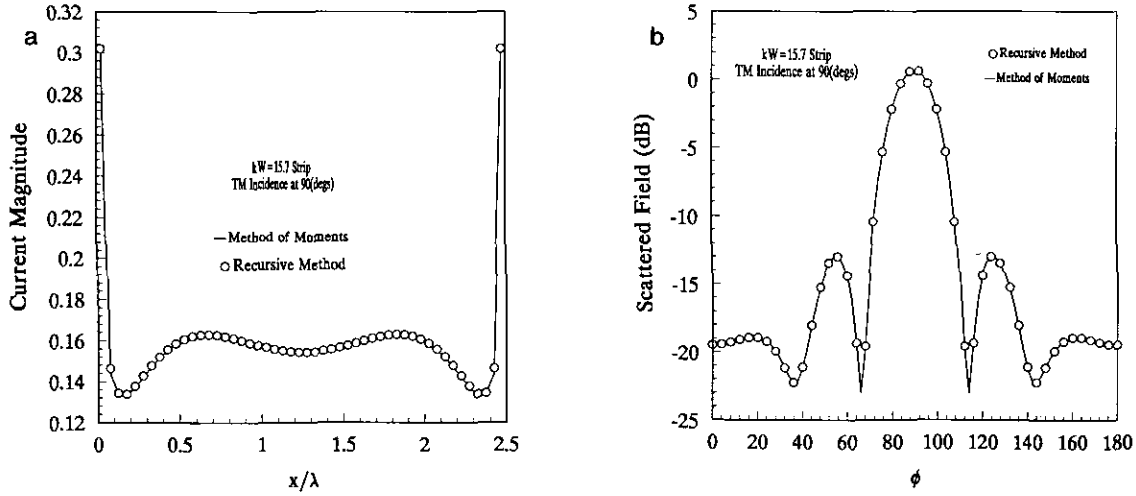


FIG. 6. A single $kW = 15.7$ strip illuminated by a TE plane wave at normal incidence, and comparison with the method of moments: (a) The current distribution on the strip. (b) The scattered far field.

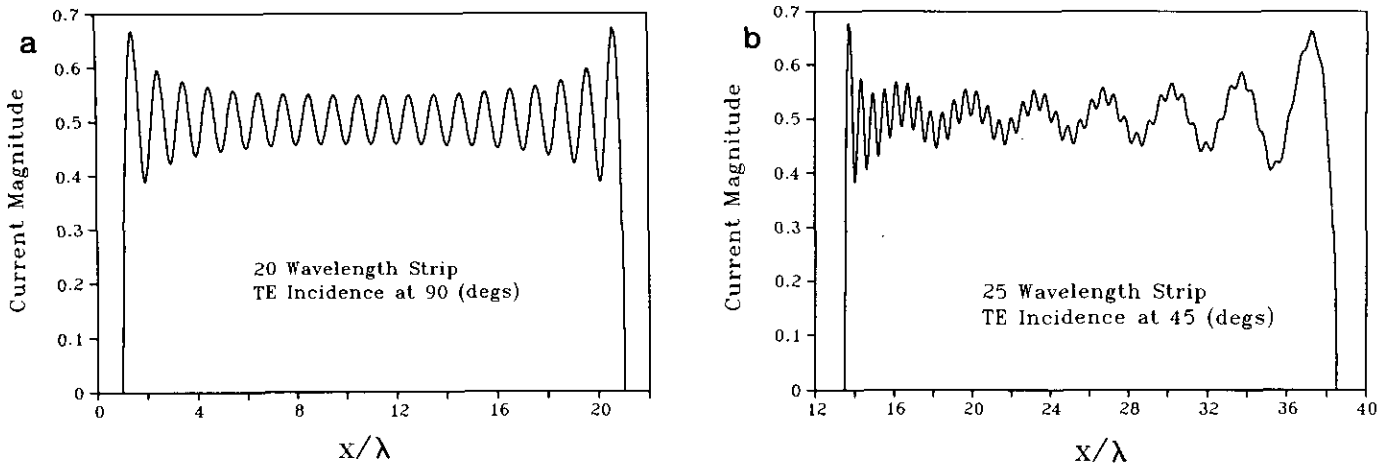


**FIG. 7.** The current distribution on: (a) a 20-wavelength wide strip illuminated by a normally incident TE plane wave; (b) a 25-wavelength strip illuminated by a TE plane wave at 45° incidence.

TE plane wave.[1] The current distribution has a small-length-scale variation on the order of a wavelength. Figure 7b shows the current distribution on a 25-wavelength strip illuminated by a 45° incident, TE plane wave. A small-scale variation on top of the large-scale variation is observed. The small-length-scale variation is due to the interference of the surface waves on the strip which bounce between the two edges of the strip. As is well known, for such a polarization, an edge-diffracted field will launch a surface wave along the strip [26]. The large-scale variation is due to the interference between the surface wave and the incident wave. In other words, the current distribution is approximately a linear superposition of three terms: $c_1 e^{ikx} + c_2 e^{-ikx} + c_3 e^{ik_{ix}x}$. The first two terms are due to surface waves bouncing between the two edges of the strip while the third term is induced by the incident wave or the physical-optics approximated current. Such interference phenomenon is not pronounced for strips illuminated by a TM polarized wave.

Figure 8 shows the current distribution on a 100-wavelength wide strip illuminated by a TE plane wave. The angle $\phi_i$ of this figure is 30°. Two length-scale variations are again observed, one at about 10-wavelength length scale and the other at one wavelength length scale. The small-scale variation is due to the interference of the surface wave as observed in the 20-wavelength example. The large-scale variation is due to the interference of the edge-diffracted field and the incident field.

Figure 9 shows the current distribution on a 160 wavelength wide strip illuminated by a TM plane wave at 45° incidence. Except near the edge, the current distribution is similar to that from physical-optics approximation. When the current near the edge is enlarged, it has an interference pattern resembling that of Fig. 6a. A metallic surface does not support well a TM-to-$z$ surface wave since $E_z$ has to be zero on the surface. Hence, the edge-diffracted field is only localized near the edge causing some interference fringes.

Figure 10 shows the growth of the CPU time on a SUN 4/110 versus the number of unknowns. The reduced computational complexity is clear from such a plot. Due to the reduced computational complexity and memory requirement, we can solve a 600-wavelength wide strip problem on a SUN 4/110 ($\simeq$1 MFLOP, 8 MByteRAM) with 6000 unknowns in about 21 min for one incident wave direction.

Even though the examples illustrated here are wide strips whose substrips are continuous, the algorithm has also been used to compute the scattering solutions for an array of

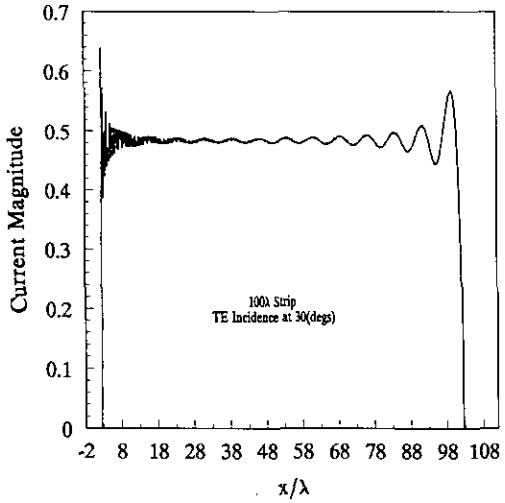


**FIG. 8.** The current distribution on a 100-wavelength wide strip illuminated by a TE plane wave with $\phi_i = 30°$ in Fig. 1.

[1] This current distribution has been validated by S. K. Jeng independently with his method-of-moments code.

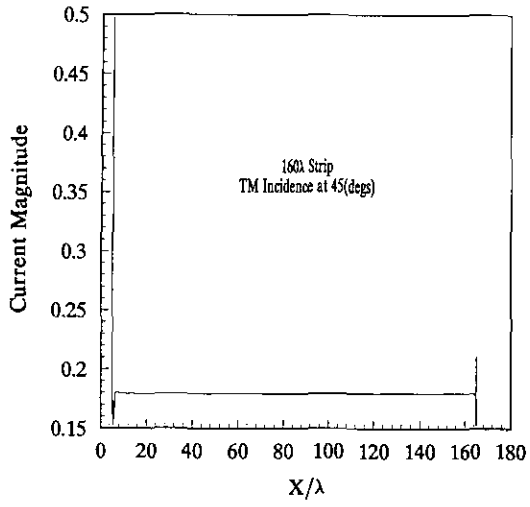


FIG. 9. The current distribution on a 160-wavelength wide strip illuminated by a TM plane wave at 45° incidence.

strips showing good agreement with the method of moments.

## 8. CONCLUSIONS

A method to calculate the scattering solutions of a wide strip or a wide array of strips is described. This method yields an accurate solution within numerical approximations, and all interactions between the substrips are accounted for. The algorithm has $N \log^2 N$ complexity for one incident angle and $N^2 \log N$ complexity for $N$ incident angles, with memory requirements of $N \log N$ and $N^2$, respectively, for the above two cases.

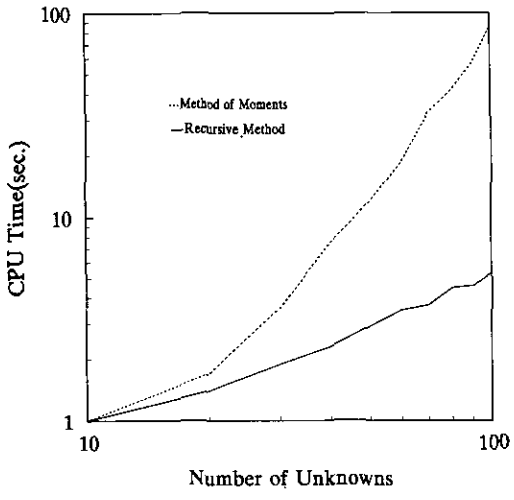


FIG. 10. Comparison of the CPU time on a SUN 4/110 versus the number of unknowns on a log–log scale.

The method has been validated with the method of moments for small strips. An interesting surface-wave interference phenomenon of the current distribution for TE polarization is observed which persists even for very large strips. This renders the physical-optics approximated current inaccurate. However, for TM polarization, this interference pattern is absent except near the edge of the strip. Hence, the physical-optics approximation is a decent one for TM polarized waves.

Even though our sampling rate for the current on the strip seems to be higher than that required for the method of moments, future research on a better choice of basis may reduce this sampling rate. However, because of the reduced complexity, the fast algorithm solves for the solution much faster than the method of moments even for one- or two-wavelength wide strips.

This work can be generalized to the case of an array of strips on a dielectric slab. We hope that future work will lift the restriction on the coplanar arrangement of the strips.

## REFERENCES

1. W. C. Chew, *Microwave Opt. Technol. Lett.* **2** (11), 380 (1989).
2. W. C. Chew, J. Friedrich, and R. Geiger, *IEEE Trans. Geosci. Remote Sensing* **28** (2), 207 (1990).
3. Y. M. Wang and W. C. Chew, *Microwave Opt. Technol. Lett.* **3** (3), 102 (1990).
4. W. C. Chew and Y. M. Wang, *Microwave Opt. Technol. Lett.* **3** (5), 164 (1990).
5. W. C. Chew, *Waves and Fields in Inhomogeneous Media* (Van Nostrand Reinhold, New York, 1990).
6. Y. M. Wang and W. C. Chew, *Microwave Opt. Technol. Lett.* **4** (4), 155 (1991).
7. L. Gurel and W. C. Chew, *Radio Sci.* **27** (3), 387 (1992).
8. W. C. Chew, L. Gurel, Y. M. Wang, G. Otto, R. Wagner, and Q. H. Liu, *IEEE Trans. Microwave Theory Technol.* **MIT-40** (4), 716 (1992).
9. W. C. Chew, Y. M. Wang, and L. Gurel, Technical Report No. EM-WC-12-91, *J. Electromag. Waves Appl.* **6** (11), 1537 (1992).
10. Y. M. Wang, Ph.D. thesis, Dept. of Elect. and Comput. Engg., UIUC, December 1990 (unpublished).
11. N. J. Vilenkin, *Special Functions and the Theory of Group Representations* (Amer. Math. Soc., Providence, RI, 1968).
12. W. K. Tung, *Group Theory in Physics*, (World Scientific, Singapore, 1984).
13. W. A. Ko and R. Mittra, *IEEE Trans. Antennas Propag.* **AP-36**, 496 (1988).
14. K. Uchida, T. Noda, and T. Matsunaga, *Electron. Commun. Jpn*, Pt. 2 **73** (8), 49 (1989).
15. R. Kastner, *IEEE Trans. Antennas Propag.* **AP-37**, 353 (1989).
16. L. Gurel and W. C. Chew, *IEEE Trans. Antennas Propag.* **AP-38**, 507 (1990).
17. C. T. Tai, *Dyadic Green's Functions in Electromagnetic Theory*, (Intext Educational, San Francisco, 1971).

18. J. A. Kong, *Electromagnetic Wave Theory* (Wiley, New York, 1986).
19. P. C. Waterman, *J. Acoust. Soc. Am.* **45**, 1417 (1969).
20. B. Peterson and S. Ström, *Phys. Rev. D* **8**, 3661 (1973).
21. A. W. Glisson and D. R. Wilton, *IEEE Trans. Antennas Propag.* **AP-28** (5) 593 (1980).
22. M. F. Catedra, *Electron. Lett.* **22**, 1049 (1986).
23. D. T. Borup, D. M. Sullivan, and O. P. Gandhi, *IEEE Trans. Microwave Theory Tech.* **MTT-35** (4), 383 (1987).
24. C. C. Su, *IEEE Trans. Antennas Propag.* **AP-35** (12), 1418 (1987).
25. C. Y. Shen, K. J. Glover, M. I. Sancer, and A. D. Varvatsis, *IEEE Trans. Antennas Propag.* **AP-37** (8), 1032 (1989).
26. G. L. James, *Geometrical Theory of Diffraction for Electromagnetic Waves* (Peregrinus, London, 1986).